ICRR-Report-676-2014-2
IPMU 14-0089

Prepared for submission to JCAP

arXiv:1404.0951v2 [astro-ph.CO] 4 Jun 2014

Curvaton in large field inflation

Tomohiro Fujita[a,b] **Masahiro Kawasaki**[c] **Shuichiro Yokoyama**[c]

[a]Kavli Institute for the Physics and Mathematics of the Universe (Kavli IPMU), TODIAS, the University of Tokyo, 5-1-5 Kashiwanoha, Kashiwa, 277-8583, Japan

[b]Department of Physics, University of Tokyo, Bunkyo-ku 113-0033, Japan

[c]Institute for Cosmic Ray Research, University of Tokyo, 5-1-5 Kashiwa-no-Ha, Kashiwa, Chiba, 277-8582, Japan

E-mail: tomohiro.fujita@ipmu.jp, kawasaki@icrr.u-tokyo.ac.jp, shu@icrr.u-tokyo.ac.jp

Abstract. We comprehensively explore the quadratic curvaton models in the chaotic inflation. In the light of the BICEP2 result $r \approx 0.2$, all model parameters and relevant observables are computed. It is found the curvaton field value is constrained into a narrow range, $\sigma_* = \mathcal{O}(10^{-2}\text{-}10^{-1})$ and the running of the spectral index is $n_s' \gtrsim -10^{-3}$. We show that if the curvaton is added, the models are heavily degenerated on the n_s - r plane. However, introducing a new plane, the degeneracy can be resolved. To distinguish the curvaton models, precise measurements of not only r but also n_s' and the tensor tilt n_T are required.

Keywords: inflation

ArXiv ePrint: 1404.0951

Contents

1 Introduction **1**

2 Implication for the curvaton scenario with the chaotic inflation **2**
2.1 Brief Review on the chaotic inflation 2
2.2 Curvaton contribution to the tensor-to-scalar ratio and the spectral index 3
2.3 Degeneracy on the n_s-r plane 5

3 Distinguish the models? **6**
3.1 Tensor tilt and the running of the spectral index of the curvature perturbations 7
3.2 Resolution of the degeneracy on the n_s'-(n_T/r) plane 9

4 Comments on non-Gaussianity and the curvaton field value **10**

5 Conclusion **12**

A The other parameters **13**

1 Introduction

The inflation paradigm is accepted as an increasingly plausible scenario of the primordial universe. Although the integrated theory that describes high energy physics including inflation is not yet identified, the candidates (e.g. the supergravity theory) predict the existence of many scalar fields and one of them can play a role of an inflaton. Since a light scalar field acquires its fluctuation during inflation, it is natural to expect that not only the inflaton but also the other scalar fields contribute to the generation of primordial cosmic perturbations. Such scenarios where the contribution of additional scalar fields to the observed perturbations are significant are known as "the curvaton-like models". In curvaton models, an additional scalar field (curvaton) has only a tiny fraction of the total energy density during inflation but its energy fraction increases after inflation and produces the curvature perturbation when it decays [1–3].

Recently, BICEP2 experiment has reported a large tensor-to-scalar ratio, $r \approx 0.2$ [4]. [1] If it is confirmed, it indicates that the Hubble parameter during inflation is $\mathcal{O}(10^{14})$GeV and the large field inflation models are strongly favored. With such a large Hubble parameter, a curvaton acquires a large fluctuation. However, an inflaton in the large field models also significantly contributes to the perturbations and their values can be explicitly computed if the inflation model is fixed. Because these perturbations generated by the two sources should be compatible with the observations, we can put strong constraints on the curvaton models.

Moreover, considering that the curvaton contribution may be relevant, it is important to find a way to determine the curvaton model in addition to the inflation model. As for the discrimination of the inflation models, the spectral index n_s and the tensor-to-scalar ratio r are useful and the n_s- r plane is frequently utilized. Once a curvaton is added, however, a wide region on the the n_s- r plane can be reproduced by various models and the plane

[1] There are related papers about curvaton scenario in the light of BICEP2 [5, 6].

is not sufficient to distinguish the curvaton models. Therefore, when curvaton models are discussed, it is necessary to investigate more observables and the verifiability of the models.

In this paper, we comprehensively explore the two curvaton models in the chaotic inflation [7, 8]. In one model, the curvaton has only its constant mass, m_σ. In the other model, the curvaton has the Hubble induced mass as well as its intrinsic mass. We investigate not only the curvaton mass and n_s but also the running n_s', the curvaton field value during inflation σ_*, the non-linear parameters $f_{\rm NL}, \tau_{\rm NL}$, its energy fraction at its decay $\hat{r}$ and its decay rate Γ_σ in the two models.

We show these curvaton models can realize a wide range of n_s and r values. Furthermore, these models are heavily degenerated on the n_s-r plane. Then we discuss the running of the scalar spectrum n_s' and a combination of r and the tilt of the tensor spectrum n_T to discriminate the curvaton models. It is demonstrated that these curvaton models are distinct on the n_s' - (n_T/r) plane. Thus we found the new plane is useful to discuss the difference between curvaton-like models in the same way as the n_s-r plane for inflation models. It is also found that the field value of the curvaton during inflation is constrained into $\mathcal{O}(10^{-2}$-$10^{-1})M_{\rm Pl}$.

The rest of this paper is organized as follows. In section 2, first we briefly review the chaotic inflation model, and then we show the implication of the curvaton scenario with the relatively large tensor-to-scalar ratio. We also mention the degeneracy of the models in 2-dimensional parameter space of the tensor-to-scalar ratio and the spectral index of the curvature perturbation. In section 3, we explore the possibility to resolve the degeneracy by introducing a new 2-dimensional parameter space. In section 4, the non-linear parameters and a constraint on the curvaton field value are calculated. Section 5 is devoted to the conclusion.

2 Implication for the curvaton scenario with the chaotic inflation

2.1 Brief Review on the chaotic inflation

In this section, we briefly review the chaotic inflation model. The inflaton potential is given by [7, 8]

$$U(\phi) = \frac{1}{p}\frac{\phi^p}{M^{p-4}}. \tag{2.1}$$

This potential can be naturally realized in the supergravity setup [9–12]. For such kind of potential, slow-roll parameters are given by

$$\begin{aligned}\epsilon &\equiv \frac{M_{\rm Pl}^2}{2}\left(\frac{U'}{U}\right)^2 = \frac{p^2 M_{\rm Pl}}{2\phi^2},\\ \eta &\equiv M_{\rm Pl}^2\frac{U''}{U} = p(p-1)\frac{M_{\rm Pl}^2}{\phi^2} = \frac{2(p-1)}{p}\epsilon,\end{aligned} \tag{2.2}$$

where a prime denotes the derivative in terms of ϕ. In the slow-roll approximation where $\epsilon, \eta \ll 1$, the e-folding number during inflation is evaluated as

$$N \simeq M_{\rm Pl}^{-2}\int_{\phi_{\rm end}}^{\phi}\frac{U}{U'}d\phi \simeq \frac{1}{2pM_{\rm Pl}^2}\left(\phi^2 - \phi_{\rm end}^2\right) = \frac{\phi^2}{2pM_{\rm Pl}^2} - \frac{p}{4}, \tag{2.3}$$

where we define the end of inflation as $\epsilon_{\rm end} = 1$. Then the slow-roll parameters are written in terms of e-folding number as

$$\epsilon = \frac{p}{4N + p}. \tag{2.4}$$

The curvature perturbation generated by the inflaton fluctuation is simply given by

$$\mathcal{P}_\zeta^{(\phi)}(k) = \left(\frac{H_*^2}{2\pi\dot{\phi}_*}\right)^2 = \frac{H_*^2}{8\pi^2\epsilon M_{\rm Pl}^2}, \tag{2.5}$$

where a dot denotes the derivative in terms of cosmic time and the subscript "$*$" denotes quantities at the horizon crossing of the mode with a corresponding wave number k while the superscript "(ϕ)" denotes quantities generated by the inflaton. By using the slow-roll parameter (or e-folding number), the spectral index n_s is also predicted as

$$n_s^{(\phi)} - 1 \equiv \frac{{\rm d}\ln\mathcal{P}_\zeta^{(\phi)}}{{\rm d}\ln k} = -2\left(\frac{2+p}{p}\right)\epsilon = -2\left(\frac{2+p}{4N+p}\right) < 0, \tag{2.6}$$

Gravitational waves are also produced during inflation and its power spectrum is predicted as

$$\mathcal{P}_g(k) = \frac{8}{M_{\rm Pl}^2}\left(\frac{H_*}{2\pi}\right)^2. \tag{2.7}$$

The ratio between $\mathcal{P}_\zeta^{(\phi)}$ and $\mathcal{P}_g$ can be simply related with the slow-roll parameter as

$$r^{(\phi)} \equiv \frac{\mathcal{P}_g}{\mathcal{P}_\zeta^{(\phi)}} = 16\epsilon. \tag{2.8}$$

2.2 Curvaton contribution to the tensor-to-scalar ratio and the spectral index

In this section, we generally consider an additional contribution to the scalar perturbation in curvaton scenario. However, we note that the results of this section are applicable to not only curvaton models but also the other type of the curvaton-like models (e.g. the modulated reheating models [13–15]).

First, according to the δN formalism [16–18], the power spectrum of the curvature perturbation which is sourced not only from the inflaton fluctuation but also the fluctuation of the additional scalar filed such as curvaton, σ, is given by [19, 20]

$$\mathcal{P}_\zeta(k) = (N_\phi^2 + N_\sigma^2)\left(\frac{H_*}{2\pi}\right)^2 \equiv (1+R)\mathcal{P}_\zeta^{(\phi)}, \tag{2.9}$$

where $N_a \equiv \partial N/\partial a (a = \phi, \sigma)$ and we define R as the ratio between $\mathcal{P}_\zeta^{(\phi)}$ and $\mathcal{P}_\zeta^{(\sigma)}$,

$$R \equiv \frac{\mathcal{P}_\zeta^{(\sigma)}}{\mathcal{P}_\zeta^{(\phi)}} = \left(\frac{N_\sigma}{N_\phi}\right)^2. \tag{2.10}$$

Note that the superscript "(σ)" denotes the contribution of the curvaton in the following sections while it can be replaced by the other sources. From the current cosmic microwave background (CMB) observations, we know the observed value of the amplitude of the scalar

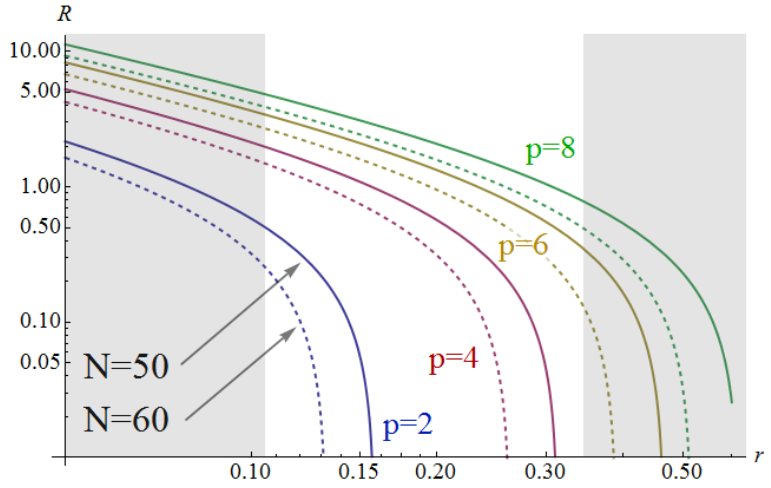

Figure 1. The ratio between the contribution to the curvature perturbation of the inflaton and that of another source, $R \equiv \mathcal{P}_\zeta^{(\sigma)}/\mathcal{P}_\zeta^{(\phi)}$. From bottom to top, the lines denote the ϕ^p models with $p = 2, 4, 6$ and 8. Solid lines and dashed lines represent the cases of $N = 50$ and $N = 60$, respectively. Grey shaded regions are excluded by BICEP2 experiment at the 2σ level.

curvature perturbation as $\mathcal{P}_\zeta = 2.2 \times 10^{-9}$ [21, 22]. On the other hand, as we have shown, the amplitude of the gravitational waves produced during inflation can be written only in terms of the inflationary Hubble parameter, H_*, as eq. (2.7) and hence the tensor-to-scalar ratio given by $r \equiv \mathcal{P}_g/\mathcal{P}_\zeta$ is directly related with H_* as

$$H_* = 1.1 \times 10^{14}\text{GeV}\sqrt{\frac{r}{0.2}}. \tag{2.11}$$

The tensor to scalar ratio in case with the additional contribution to the scalar perturbation due to the curvaton fluctuation is predicted as

$$r = \frac{r^{(\phi)}}{1+R} = \frac{16\epsilon}{1+R} \quad \Longleftrightarrow \quad R = \frac{16}{r}\left(\frac{p}{4N+p}\right) - 1. \tag{2.12}$$

Therefore the fraction of the curvaton contribution, R, is fixed by r, p and N. In fig. 1, we plot R as a function of r for each p and N. One can see that R has a finite value in a limited range of r depending on p. This is because r always decreases from $r^{(\phi)}$ due to a positive R and $r \geq r^{(\phi)}$ cannot be realized [2]. In other words, with an additional contribution to $\mathcal{P}_\zeta$, r is smaller than the prediction of the single slow-roll case;

$$R > 0 \quad \Longrightarrow \quad r < r^{(\phi)} = 16\epsilon. \tag{2.13}$$

Here we list the upper bound on r where the curvaton can work,

$$N = 50: \quad r^{(\phi)}_{(p=2)} = 0.16, \quad r^{(\phi)}_{(p=4)} = 0.31, \quad r^{(\phi)}_{(p=6)} = 0.46, \quad r^{(\phi)}_{(p=8)} = 0.62, \tag{2.14}$$

$$N = 60: \quad r^{(\phi)}_{(p=2)} = 0.13, \quad r^{(\phi)}_{(p=4)} = 0.26, \quad r^{(\phi)}_{(p=6)} = 0.39, \quad r^{(\phi)}_{(p=8)} = 0.52. \tag{2.15}$$

[2] See, however, ref. [23] in which the realization of a negative R by a curvaton is discussed.

Next, let us focus on the spectral index of the scalar curvature perturbations. In order to investigate the spectral index, we need to specify the potential for the curvaton-like field which gives the additional contribution to the curvature perturbations. Here, we consider the following two models of curvaton,

$$V_H(\sigma) = \tfrac{1}{2}cH^2\sigma^2, \qquad V_I(\sigma) = \frac{1}{2}m_\sigma^2\sigma^2. \tag{2.16}$$

In the former model, we consider the Hubble induced mass (HIM) [24, 25]. Note that during inflation, a scalar field generally acquires the HIM through the supergravity effect which is originated from the breaking of supersymmetry due to the inflation energy density [26, 27]. A parameter which characterizes the amplitude of HIM, c, is a constant during inflation, $c = c_i$, but it takes a different value in the successive matter dominant (inflaton oscillation) era and the radiation dominant era [28–30] [3]. We assume that both c_iH^2 and m_σ^2 are much smaller than H^2 during inflation, in order for σ to acquire quantum fluctuations as $\mathcal{P}_{\delta\sigma}(k) = (H_*/2\pi)^2$ in both cases. Then, the spectral index of the curvature perturbation for such case is calculated as [20]

$$n_s - 1 = -\frac{1}{1+R}\frac{2(2+p)}{4N+p} + \frac{R}{1+R}\left[-2\epsilon + \frac{2m_{\sigma,\mathrm{eff}}^2}{3H_*^2}\right], \tag{2.17}$$

where $m_{\sigma,\mathrm{eff}}^2$ denotes $c_iH_*^2$ or m_σ^2 depending on the models. It can be easily checked that for $R \to \infty$ the pure curvaton result and for $R \to 0$ the pure inflaton result are reproduced. It should be noted that if $m_{\sigma,\mathrm{eff}}^2$ is positive (negative), it makes the spectral index bluer (redder). By solving eq. (2.17) with respect to $m_{\sigma,\mathrm{eff}}^2$ and using eqs. (2.4) and (2.12), one obtains the curvaton mass as

$$m_{\sigma,\mathrm{eff}}^2 = \frac{3}{2}\left(n_s - 1 + \frac{2p}{4N+p} + \frac{r}{4p}\right)\left(1 - \frac{r(4N+p)}{16p}\right)^{-1} H_*^2. \tag{2.18}$$

The r.h.s in eq. (2.18) contains only the observables (n_s, r, H_*) and the inflation model parameters (p, N). Thus the curvaton mass can be determined by the present observation results if the inflation model is fixed. In fig. 2, c_i and m_σ are plotted. Although the HIM and the intrinsic mass work in the similar ways, only the former squared can be negative and help the chaotic inflation models which predict larger (bluer) tilts than the observation. Therefore, in the right panel of fig. 2, the $p = 2$ case does not appear and the $p = 4$ and $N = 60$ (dashed line) case cannot has a finite m_σ for $r < 0.12$. On the other hand, the $p = 2$ lines rapidly drops in the left panel because the additional contribution to the scalar curvature perturbation can work only for $r < r^{(\phi)}$.

2.3 Degeneracy on the n_s-r plane

It is known well that the n_s - r plane is useful to distinguish single slow-roll inflation models. Especially, the prediction of the chaotic inflation model can be expressed as a definite point on the plane if the e-folding number N_* is given. Therefore the constraint on the plane is a powerful way to favor or exclude the model. However, if the curvaton is added to the chaotic

[3] In order for the curvaton to oscillate later, it also has its intrinsic mass even in the HIM model while the intrinsic mass is assumed to be negligible compared with the HIM during inflation. It is known that the parameter c during the radiation dominated era is typically $\mathcal{O}(10^{-3} - 10^{-2})$ [28–30] and hence not the Hubble induced mass but the intrinsic mass m_σ drives the curvaton oscillation, $H_{\mathrm{osc}} \simeq m_\sigma$.

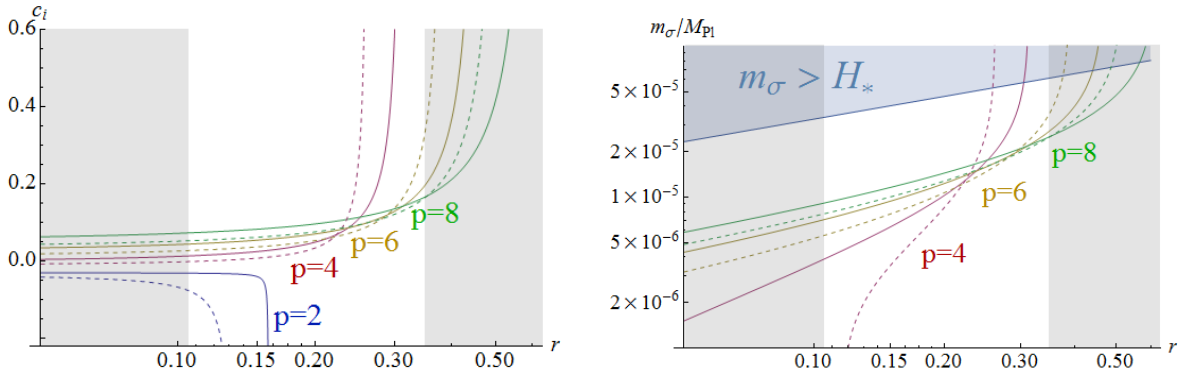

Figure 2. The left panel shows the coefficient of the HIM c_i in the model with $V_H(\sigma)$. The right panel shows the intrinsic mass m_σ in the model with $V_I(\sigma)$. The spectrum index $n_s - 1 = -0.04$ is used. The e-folding number N is 50 (solid lines) and 60 (dashed lines). In the blue shaded region, the intrinsic mass of σ exceeds H_*. The $p = 2$ line does not appear in the right panel because a positive m_σ^2 gives only a bluer spectral index than the single-field case. For the same reason, in cases with $p = 4, N = 60$, the additional contribution to the curvature perturbations in the case with only m_σ^2 cannot work for $r < 0.12$.

inflation, since the curvaton mass $m^2_{\sigma,\rm eff}$ during inflation and its relative contribution to the curvature perturbation R are the additional parameters, the model prediction occupies a finite region on the n_s-r plane. One can eliminate R from eqs.(2.12) and (2.17) and obtains,

$$\Delta r = -\frac{16p\epsilon}{4\epsilon + 2p\eta_\sigma}\Delta n_s, \qquad \left(\Delta r \equiv r - r^{(\phi)} < 0, \quad \Delta n_s \equiv n_s - n_s^{(\phi)}, \quad \eta_\sigma \equiv \frac{m^2_{\sigma,\rm eff}}{3H_*^2}\right). \tag{2.19}$$

This equation describes how the curvaton can change the prediction for $\{n_s, r\}$ of the original ϕ^p chaotic inflation models. If the curvaton mass is negligible ($\eta_\sigma \to 0$), one finds $\Delta r = -4p\Delta n_s$. A finite curvaton mass changes the gradient of the line. For $\eta_\sigma < -2\epsilon/p$, the gradient becomes positive. Note since R is positive in our scenario, Δr is always negative. Fig. 3 shows the region where the curvaton models in the chaotic inflation can access on the $\{n_s, r\}$ plane. Since in the HIM model the curvaton has a negative mass squared the accessible region is larger than the intrinsic mass model. The figure indicates that the models are heavily degenerated especially in the observationally favored region.

Let us stress that the results of this section are applicable to not only curvaton models but also the other type of the curvaton-like models.

3 Distinguish the models?

In the previous section, we mention that mixed scenarios, where both of the curvaton and inflation fluctuations contribute to the curvature perturbation, are degenerate in n_s - r plane known as a useful parameter space to distinguish single slow-roll inflation models. Hence, here we investigate a new parameter space where we would distinguish such mixed scenarios.

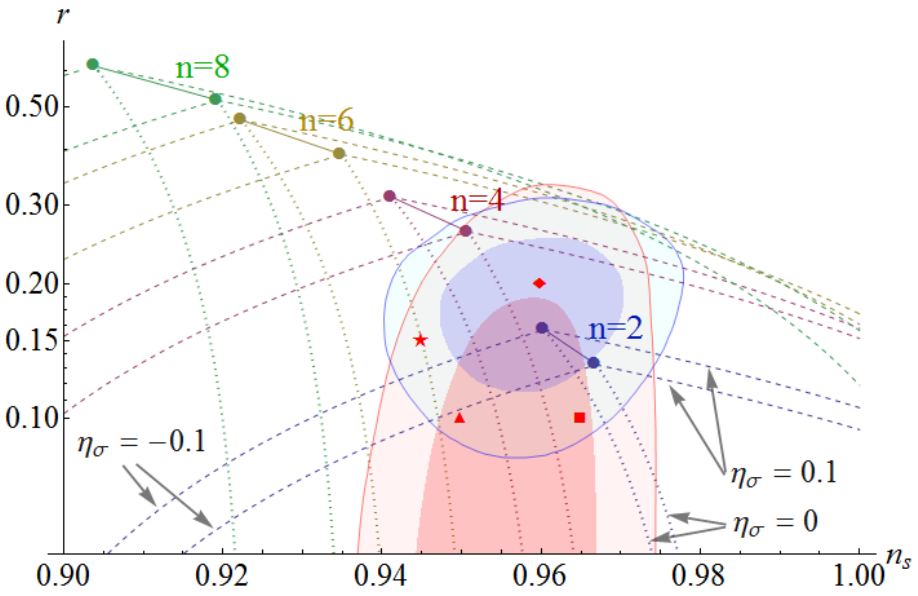

Figure 3. The accessible region of the quadratic curvaton models in the ϕ^p chaotic inflation. The pairs of circles represent the prediction of the original chaotic models for $N = 50$ (left) $N = 60$ (right). The curvaton with appropriate $R > 0$ and $|\eta_\sigma| < 0.1$ can produce $\{n_s, r\}$ in the region below the dashed lines. Since the dotted lines denote the case of $\eta_\sigma = 0$, only the curvaton with a negative mass squared generates the region to the left of the dotted lines. Blue and red shaded regions represent BICEP2 and Planck constraints, respectively [4]. For example, the point of the red star, $\{n_s, r\} = \{0.945, 0.15\}$, cannot be realized by the $p = 2$ chaotic + curvaton model, but the $p = 4$ model with a negative mass square curvaton and the $p = 6, 8$ model with a positive mass curvaton can reproduce it. One can see that in the observationally favored region, the models are heavily degenerated.

3.1 Tensor tilt and the running of the spectral index of the curvature perturbations

First, let us consider the tensor tilt n_T. Taking the derivative of eq. (2.7), one finds

$$n_T \equiv \frac{\mathrm{d}\ln \mathcal{P}_g}{\mathrm{d}\ln k} = -2\epsilon. \tag{3.1}$$

Combining the above expression for n_T with eq. (2.8), we obtain so-called "the consistency relation" of single slow-roll inflation models as [31]

$$r^{(\phi)} = -8n_T. \tag{3.2}$$

On the other hand, once the additional contribution to the curvature perturbations exists, the tensor-to-scalar ratio is modified as shown in the previous section and hence the above consistency relation would be violated as

$$r = \frac{r^{(\phi)}}{1+R} = \frac{-8n_T}{1+R}. \tag{3.3}$$

In other words, through the above expression, R can be observationally determined by the combination of the tilt of the tensor spectrum n_T and the tensor-to-scalar ratio r as

$$R = -1 - 8\frac{n_T}{r}. \tag{3.4}$$

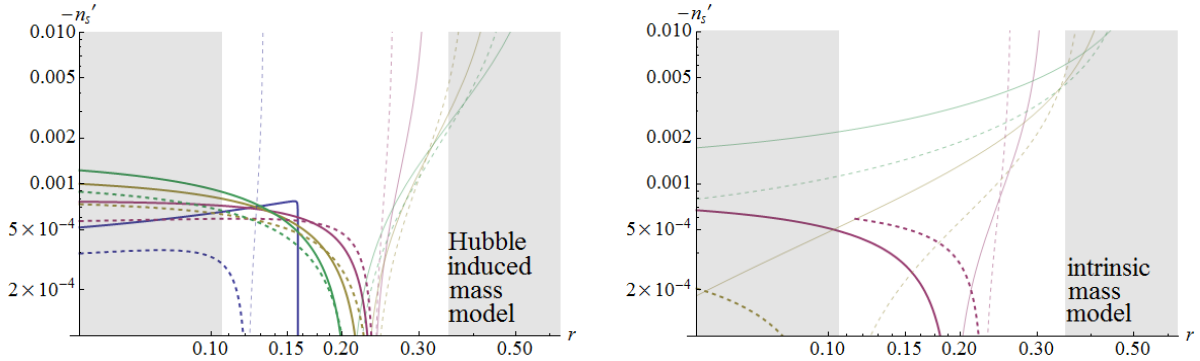

Figure 4. The running of the spectrum index n_s' in the HIM model (left panel) and the intrinsic mass model (right panel). The vertical axis is $-n_s'$ while transparent lines represent positive n_s'. The colors denotes the inflation model as $p = 2$ (blue), 4 (red), 6 (yellow) and 8 (green). The e-folding number N is 50 (solid lines) and 60 (dashed lines). $n_s = 0.96$ is used to fix the curvaton (effective) mass. The magnitude of the negative running is less than 10^{-3} while the positive running can be larger.

On the other hand, the running of the spectral index of the curvature perturbation in the standard single slow-roll inflation is given by[4]

$$n_s'^{(\phi)} \equiv \frac{\mathrm{d}n_s^{(\phi)}}{\mathrm{d}\ln k} = -8\left(\frac{2+p}{p^2}\right)\epsilon^2 = -8\frac{(2+p)}{(4N+p)^2} < 0, \tag{3.5}$$

and we also obtain the running in the case with the additional contribution from the curvaton fluctuation as [5]

$$\begin{aligned} n_s'(m_\sigma) &= -\frac{8}{1+R}\left[\frac{2+p}{p^2}\epsilon^2\right] + \frac{R}{1+R}\left[-\frac{8}{p}\epsilon^2 + \frac{4m_\sigma^2}{3H^2}\epsilon\right] + \frac{R}{(1+R)^2}\left[\frac{4}{p}\epsilon + \frac{2m_\sigma^2}{3H^2}\right]^2, \\ n_s'(c_i) &= -\frac{8}{1+R}\left[\frac{2+p}{p^2}\epsilon^2\right] + \frac{R}{1+R}\left[-\frac{8}{p}\epsilon^2\right] + \frac{R}{(1+R)^2}\left[\frac{4}{p}\epsilon + \frac{2}{3}c_i\right]^2, \end{aligned} \tag{3.6}$$

where $n_s'(m_\sigma)$ denotes the model with the intrinsic mass, m_σ, while $n_s'(c_i)$ denotes the model with the HIM, $c_i H_*^2$, during inflation. The first, the second and the third term represent the contributions from the inflaton, the curvaton and their mixture, respectively. Notice the second term has the extra term in the former model because in the latter model, $m_{\sigma,\mathrm{eff}}^2/H_*^2$ is constant and its derivative vanishes.

Fig. 4 shows n_s' in the case with the Hubble induced mass (left panel) and the intrinsic mass (right panel). The mass of the curvaton, $m_{\sigma,\mathrm{eff}}^2$, would be determined by the observables with fixing the inflation model as shown in Eq. (2.18), and hence from the expression (3.6), n_s' can be also written in terms of the observables (n_s, r, H_*) and the inflationary parameter (p, N). As shown in Eq. (3.6), since terms originated from the mass of the curvaton σ always have the positive contributions to n_s', they somewhat cancel the negative contribution from the inflaton which is proportional to ϵ^2. Thus when n_s' is negative, its magnitude is comparable or smaller than the original prediction of the inflation and it means that the

[4] When one computes the derivatives of the slow-roll parameters, $\mathrm{d}\epsilon/\mathrm{d}\ln k = 2\epsilon(2\epsilon - \eta) = 4\epsilon^2/p$ is useful.

[5] One can show useful equations, $\frac{\mathrm{d}\ln R}{\mathrm{d}\ln k} = \frac{4}{p}\epsilon + \frac{2m_{\sigma,\mathrm{eff}}^2}{3H^2}$ and $-\frac{\mathrm{d}}{\mathrm{d}\ln k}\frac{1}{1+R} = \frac{\mathrm{d}}{\mathrm{d}\ln k}\frac{R}{1+R} = \frac{R^2}{(1+R)^2}\left[\frac{4}{p}\epsilon + \frac{2m_{\sigma,\mathrm{eff}}^2}{3H^2}\right]$.

maximum absolute value of the negative n_s' is given by $n_s'^{(\phi)}$ listed as

$$N = 50: \quad n_{s(p=2)}'^{(\phi)} = -7.8 \times 10^{-4}, \quad n_{s(p=4)}'^{(\phi)} = -1.1 \times 10^{-3} \tag{3.7}$$

$$n_{s(p=6)}'^{(\phi)} = -1.5 \times 10^{-3}, \quad n_{s(p=8)}'^{(\phi)} = -1.8 \times 10^{-3}, \tag{3.8}$$

$$N = 60: \quad n_{s(p=2)}'^{(\phi)} = -5.5 \times 10^{-4}, \quad n_{s(p=4)}'^{(\phi)} = -8.1 \times 10^{-3} \tag{3.9}$$

$$n_{s(p=6)}'^{(\phi)} = -1.1 \times 10^{-3}, \quad n_{s(p=8)}'^{(\phi)} = -1.3 \times 10^{-3}. \tag{3.10}$$

3.2 Resolution of the degeneracy on the n_s'-(n_T/r) plane

As shown in the previous subsection, the ratio n_T/r fixes the relative contribution of the curvaton or the other additional degrees of freedom (see eq. (3.4)). In other words, it implies how the observed r deviates from the original prediction of a inflation model, namely "the consistency relation". Therefore if observations fix both r and n_T with sufficient accuracy, the most favored inflation model at least in the light of the tensor perturbation is determined without an uncertainty from curvaton-like models. However, the curvaton model is not identified because various curvaton models (e.g. the HIM model or the intrinsic mass model) can produce the same amount of R.

Then we need another observable to distinguish curvaton models. The running of the spectrum index n_s' can be useful for the purpose. As we see in fig. 4, n_s' predicted by models are different and can work as a discriminator. This is because the parameters in curvaton models are fixed to reproduce the observed n_s. Thus the differences between models appear in the prediction for n_s'.

Let us consider the plane whose x-axis is n_s' and y-axis is $R = -1 - 8n_T/r$. Using eqs. (2.12), (2.17) and (3.6), the location on the $\{n_s', R\}$ plane can be described by n_s and r. In the two curvaton models, the expressions of n_s' are given by

$$\begin{aligned} n_s'(m_\sigma) &= 2\epsilon(n_s - 1 + 2\epsilon) + \frac{\epsilon}{2p}(r - 16\epsilon) - \frac{r\epsilon}{p^2} - \frac{rp^{-2}}{r - 16\epsilon}\left[4\epsilon + p(n_s - 1 + 2\epsilon)\right]^2, \\ n_s'(c_i) &= \frac{p^2 r(n_s + 2\epsilon - 1)^2 + 8p\epsilon\left(r(n_s + 3\epsilon - 1) - 16\epsilon^2\right) + r^2\epsilon}{p^2(16\epsilon - r)}, \end{aligned} \tag{3.11}$$

where $\epsilon = p/(4N + p)$ in the chaotic inflation model.

In fig. 5 and fig. 6, we demonstrate that the two curvaton models in the ϕ^p chaotic inflation are distinguishable on the new plane. These figures should be compared with fig. 3. The deviations between the original predictions of the inflation models and the fiducial points (we adopt $\{n_s, r\} = \{0.945, 0.15\}, \{0.95, 0.1\}, \{0.96, 0.2\}$ and $\{0.965, 0.1\}$, see the red points in fig. 3) reflect the differences on the n_s'-R plane. It should be noted that the consistency relation is satisfied on the x-axis of the n_s'-R plane, namely $R = 0$.

Regarding observations, in order to discriminate the curvaton models, typically $\mathcal{O}(10^{-4})$ accuracy in the determination of n_s' is required. Such a great accuracy may be still challenging in the next generation observations [32, 33]. For example, in ref. [33], the authors argue that 1σ uncertainty for n_s' is larger than 10^{-4} even from a combination of CMB and 21cm fluctuation future experiments (i.e. CMBpol + Omniscope). Thus a more advanced observation is required to distinguish the curvaton models.

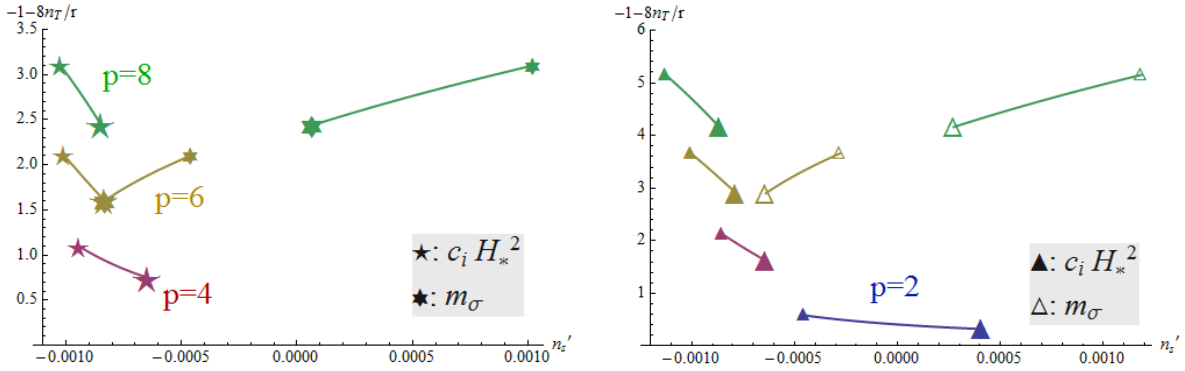

Figure 5. The left panel shows the model predictions for $\{n_s, r\} = \{0.945, 0.15\}$ (the red star in fig. 3) while the right panel shows the case with $\{n_s, r\} = \{0.95, 0.1\}$ (the red triangle in fig. 3). The smaller symbols denote the $N = 50$ cases and bigger ones denote the $N = 60$ cases. One can see that model predictions are distinct from each other. Only in the case of $p = 6$, two models converge because the curvaton mass is negligible there (see fig. 3).

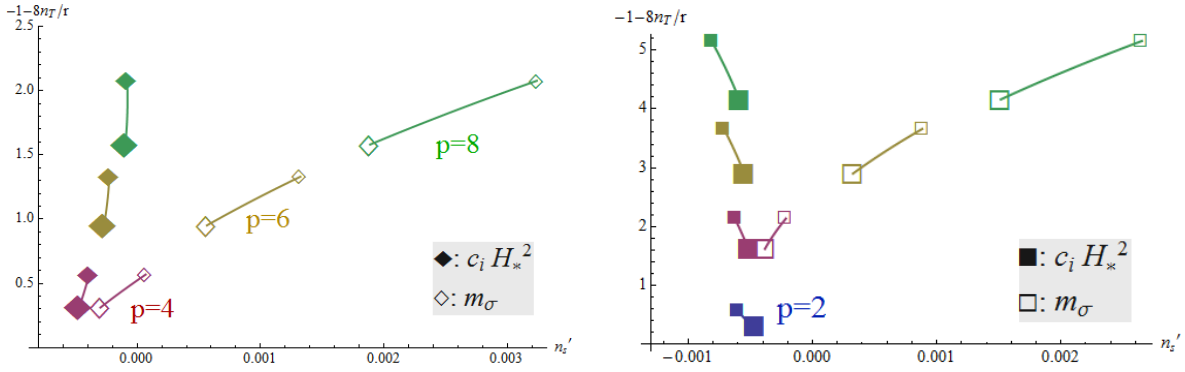

Figure 6. The left panel shows the case with $\{n_s, r\} = \{0.96, 0.2\}$ (the red diamond in fig. 3) while the right panel shows the case with $\{n_s, r\} = \{0.965, 0.1\}$ (the red spade).

4 Comments on non-Gaussianity and the curvaton field value

In this section we discuss the non-linearity parameters and the curvaton field value σ_*. In curvaton models with a quadratic potential, the non-linearity parameters are given by [19, 20]

$$f_{\rm NL} \simeq \frac{5}{6}\left(\frac{R}{1+R}\right)^2 \frac{N_{\sigma\sigma}}{N_\sigma^2} = \frac{5}{12}\left(\frac{R}{1+R}\right)^2 \left[-3 + \frac{4}{\hat{r}} + \frac{8}{4+3\hat{r}}\right], \tag{4.1}$$

$$\tau_{\rm NL} \simeq \left(\frac{R}{1+R}\right)^3 \left(\frac{N_{\sigma\sigma}}{N_\sigma^2}\right)^2 = \left(\frac{1+R}{R}\right)\left(\frac{6}{5} f_{\rm NL}\right)^2, \tag{4.2}$$

where $\hat{r}$ is defined as the ratio between the radiation energy density ρ_γ and the curvaton energy density ρ_σ at the time of the curvaton decay:

$$\hat{r} \equiv \frac{\rho_\sigma}{\rho_\gamma}(t_{\sigma,\rm dec}), \tag{4.3}$$

and the contributions to the non-linearity parameters from the inflaton are ignored because they are suppressed by the slow-roll parameters. Note that $f_{\rm NL}$ and R should be considered

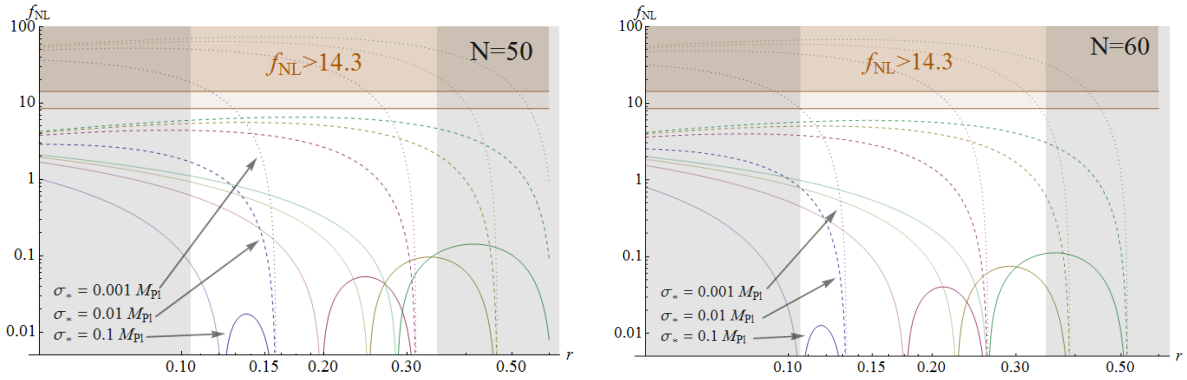

Figure 7. $f_{\rm NL}$ for varying σ_*. The solid, dashed and dotted lines represent $\sigma_* = 10^{-1}, 10^{-2}$ and $10^{-3} M_{\rm Pl}$, respectively. The transparent solid lines represent negative $f_{\rm NL}$ values. The colors denotes the chaotic inflation model of $p = 2$ (blue), 4 (red), 6 (yellow) and 8 (green). The e-folding number is $N = 50$ (left panel) and $N = 60$ (right panel). The brown (light brown) shaded regions are excluded by the Planck observation at the 2σ (1σ) level.

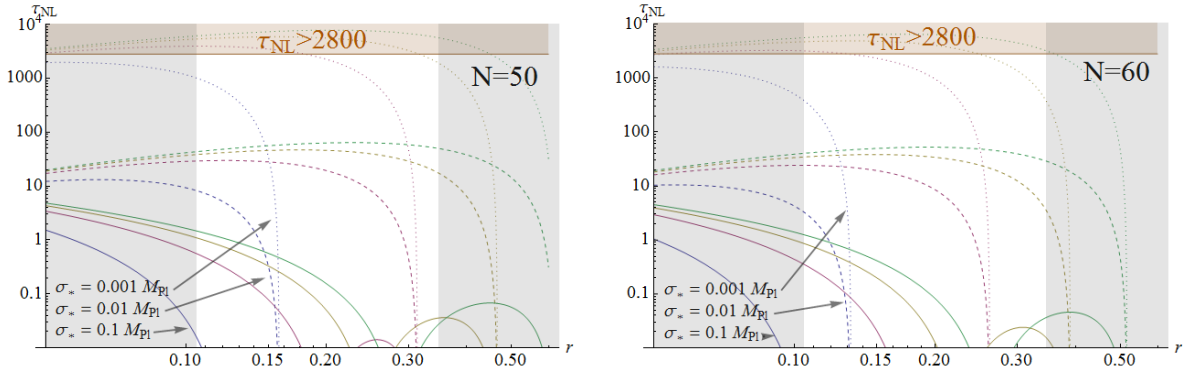

Figure 8. $\tau_{\rm NL}$ for varying σ_*. All colors and plot styles have the same meaning as fig. 7.

together because they are functions of $\hat{r}$. In terms of $\hat{r}$, the parameter R is given by [34, 35]

$$R = \left(\frac{2\hat{r}}{4+3\hat{r}}\right)^2 \frac{2\epsilon M_{\rm Pl}^2}{\sigma_*^2}. \tag{4.4}$$

Since $\hat{r}$ is positive and hence $2\hat{r}/(4+3\hat{r}) < 2/3$, an upper bound on σ_* can be derived as,

$$\frac{\sigma_*}{M_{\rm Pl}} < \frac{2}{3}\sqrt{\frac{2\epsilon}{R}}, \tag{4.5}$$

The reason why the upper limit on σ_* is obtained is that a larger σ_* leads to a smaller $\mathcal{P}_\zeta^{(\sigma)}$ which is inadequate even if the curvaton dominates the universe, $\hat{r} \to \infty$. By eliminating $\hat{r}$ from eqs. (4.1) and (4.4), we obtain

$$f_{\rm NL} = \frac{5}{12}\left(\frac{R}{1+R}\right)^2 \left[-4 + \frac{2M_{\rm Pl}}{\sigma_*}\sqrt{\frac{2\epsilon}{R}} - \frac{3\sigma_*}{M_{\rm Pl}}\sqrt{\frac{R}{2\epsilon}}\right], \tag{4.6}$$

$$\frac{\sigma_*}{M_{\rm Pl}} = \sqrt{\frac{2\epsilon}{R}}\left[\frac{R^{-2}}{15}\sqrt{36(1+R)^4 f_{\rm NL}^2 + 120R^2(1+R)^2 f_{\rm NL} + 250R^4} - \frac{2}{5}\left(\frac{1+R}{R}\right)^2 f_{\rm NL} - \frac{2}{3}\right].$$

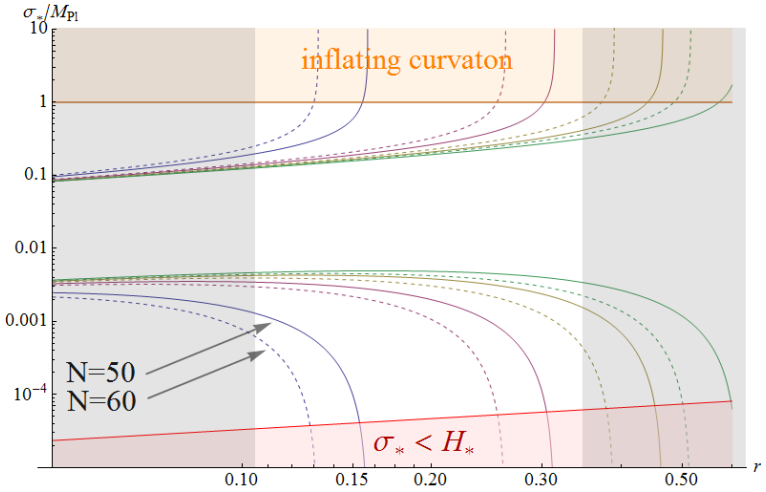

Figure 9. The regions between the pairs of the same colored lines are allowed for σ_*. The upper limits is coming from eq. (4.5) and the lower limit is originated from eq. (4.6) with $f_{\rm NL} > 14.3$. The constraints are relaxed where R becomes tiny. However the conditions for the validity of the perturbation $\sigma_* > H_*$ and the non-inflating curvaton $\sigma_* < M_{\rm Pl}$ do not allow an arbitrary value of σ_* for any r.

This pair of equations are useful in two ways. First, $f_{\rm NL}$ (and hence $\tau_{\rm NL}$) is given if σ_* and a inflation model are fixed. Second, since σ_* decreases as $f_{\rm NL}$ increases, the lower bound on σ_* can be obtained from the Planck constraint on $f_{\rm NL}$ [22]. [6]

In fig. 7 and fig. 8, we plot $f_{\rm NL}$ and $\tau_{\rm NL}$ for varying σ_*. In the chaotic inflation, σ_* is naturally expected to be lower than $M_{\rm Pl}$. This is because in the initial condition of the chaotic inflation, a light scalar field can take a large value that is even more than $M_{\rm Pl}$ [7, 8], but if $\sigma_* \gtrsim M_{\rm Pl}$, σ becomes not a curvaton but an inflaton. Therefore the cases with $\sigma_* = 10^{-1}M_{\rm Pl}, 10^{-2}M_{\rm Pl}$ and $10^{-3}M_{\rm Pl}$ are shown in those figures. Basically, a larger non-linearity are produced by a smaller σ_*. However, due to the Planck constraint $f_{\rm NL} < 14.3$ and $\tau_{\rm NL} < 2800$ at the 2σ level, σ_* which is less than $10^{-3}M_{\rm Pl}$ is excluded expect for the narrow range of r. This result is consistent with fig. 9.

Combining eqs. (4.5) and (4.6) with $f_{\rm NL} < 14.3$, we obtain the allowed value of σ_*. That is plotted in fig. 9. In the figure, one can see that σ_* is typically restricted into one or two orders of magnitude. Nevertheless the allowed value around $10^{-2}M_{\rm Pl}$ does not need a extreme fine-tuning in the context of the chaotic inflation.

5 Conclusion

In this paper, we comprehensively investigate the curvaton model with the quadratic potential in the chaotic inflation models whose potentials are ϕ^p with $p = 2, 4, 6$ and 8. With the observation of the tensor-to-scalar ratio r by BICEP2 experiment, the contribution of a curvaton-like component to the scalar perturbation can be calculated in the model-independent manner (fig. 1). Specifically we consider the two models of curvaton, that the Hubble induced mass

[6] it is interesting to note that by combining eqs. (4.5) and (4.6), one can find the lower bound on $f_{\rm NL}$ as $f_{\rm NL} > (5/12)(R/(1+R))^2 \left[\sqrt{R/2\epsilon} - 3\right]$.

curvaton model and the intrinsic mass curvaton model. Then the curvaton mass is also computed (fig. 2).

Although the two parameter space of n_s and r is useful to discriminate inflation models, we show the two curvaton models in the chaotic inflation models are heavily degenerated on the plane (fig. 3). However, it is found that the running of the spectrum index n_s' are different between the two models (fig. 4). This is because the model parameter (i.e. the curvaton mass) is fixed by the spectrum index. Moreover, the inflation models can be well determined by the observation of the tensor tilt n_T. Since n_T is given only by the inflation dynamics, the ratio of n_T and r, or "the consistency relation", implies the amount of the additional contribution from the curvaton. Therefore, introducing the new 2 parameter space of n_s' and n_T/r, we demonstrate the degeneracy of the two curvaton models can be resolved (fig. 5, 6). To distinguish the curvaton models, a precise measurement of n_s' with an $\mathcal{O}(10^{-4})$ uncertainty is required.

We also calculate the non-linearity parameters in the light of BICEP2 result (fig. 7, 8). Since $f_{\rm NL}$ increases as the curvaton field value during inflation σ_* decreases and Planck satellite put the upper bound on it, $f_{\rm NL} < 14.3$, the upper bound on σ_* is obtained. On the other hand, δN induced by the curvaton modulation decreases as σ_* increases and the curvaton contribution is fixed by r, the lower bound on σ_* is also obtained. We found that σ_* is constrained into a narrow range, but its value $\sim 10^{-2} M_{\rm Pl}$ is natural in the chaotic inflation (fig. 9).

Acknowledgments

We would like to thank Ryusuke Jinno for his useful comments. This work is supported by Grant-in-Aid for Scientific research from the Ministry of Education, Science, Sports, and Culture (MEXT), Japan, No. 25400248 (M.K.), No. 21111006 (M.K.) and the World Premier International Research Center Initiative (WPI Initiative), MEXT, Japan. T.F. and S.Y. acknowledge the support by Grant-in-Aid for JSPS Fellows No. 248160 (TF) and No. 242775 (SY).

A The other parameters

In this appendix, we discuss the remaining model parameters, namely $\hat{r}, \sigma_*$ and m_σ/Γ_σ. They are fixed if $f_{\rm NL}$ and r as well as p and N are given.

First let us calculate $\hat{r}$. By solving eq. (4.1) with respect to $\hat{r}$, we can obtain the expression of $\hat{r}$ as

$$\hat{r} = \frac{4}{9}\frac{\sqrt{36 f_{\rm NL}^2 (R+1)^4 + 120 f_{\rm NL}(R+1)^2 R^2 + 250 R^4} - 6 f_{\rm NL}(R+1)^2 + 5R^2}{4 f_{\rm NL}(R+1)^2 + 5R^2}. \tag{A.1}$$

In fig. 10, $\hat{r}$ is shown for $f_{\rm NL} = 2.7, 8.5$ and 14.3. In the pure curvaton case ($R \to \infty$ in eq. (4.1)), one obtains the lower bound on $\hat{r}$ as

$$f_{\rm NL} = \frac{5}{12}\left[-3 + \frac{4}{\hat{r}} + \frac{8}{4+3\hat{r}}\right] < 14.3 \quad \Longrightarrow \quad \hat{r} > 0.11, \qquad (R \gg 1). \tag{A.2}$$

However, in the mixed case, since the R factor in eq. (4.1) changes the $\hat{r}$ dependence, a small $\hat{r}$ (< 0.11) is allowed and the curvaton does not have to almost dominate the universe.

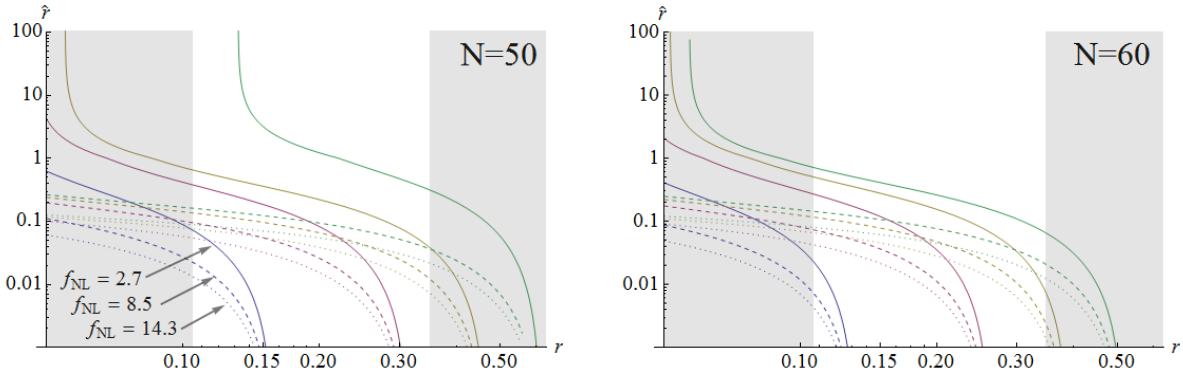

Figure 10. The plot of $\hat{r} \equiv \rho_\sigma/\rho_\gamma(t_{\sigma,\rm dec})$. The colors denotes the chaotic inflation model of $p = 2$ (blue), 4 (red), 6 (yellow) and 8 (green). The e-folding number is $N = 50$ (left panel) and $N = 60$ (right panel). Contrary to the pure curvaton case, $\hat{r}$ can be smaller than 0.1 when the curvaton contribution is less than the inflaton's ($R \lesssim 1$).

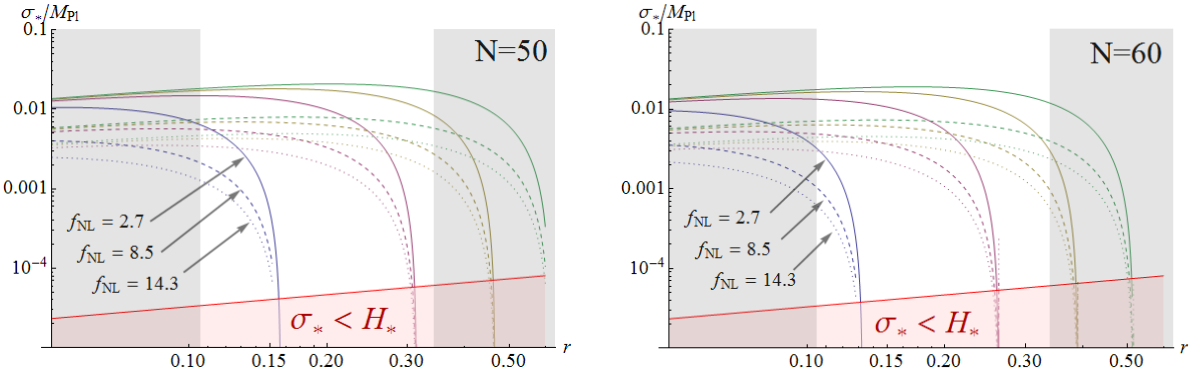

Figure 11. The σ_* value computed from the observables (i.e. $\mathcal{P}_\zeta, r$ and $f_{\rm NL}$) and the inflation model (i.e. ϕ^p chaotic inflation for $n = 2, 4, 6$ and 8 from bottom to top). The e-folding number is $N = 50$ (left panel) and $N = 60$ (right panel). The solid, dashed, dotted lines represent $f_{\rm NL} = 2.7, 8.5, 14.3$, respectively. In the red shaded region, the perturbation of the curvaton is not reliable. The dotted lines ($f_{\rm NL} = 14.3$) can be understood as the lower bound on σ_*. σ_* is typically smaller than the Planck scale by a few orders of magnitude. .

Second, let us see the value of σ_*. It is given in eq. (4.6) as the function of $f_{\rm NL}$. In fig. 11, σ_* is plotted for varying $f_{\rm NL}$. It is a counterpart of fig. 7.

Finally, the ratio between the curvaton intrinsic mass and its decay rate is also written as a function of $f_{\rm NL}$. It is known that $\hat{r}$ is given by [35] [7]

$$\hat{r} \simeq \frac{V(\sigma_{\rm osc})}{3M_{\rm Pl}^2 H_{\rm osc}^2}\sqrt{\frac{m_\sigma}{\Gamma_\sigma}} \simeq \frac{\sigma_*^2}{6M_{\rm Pl}^2}\sqrt{\frac{m_\sigma}{\Gamma_\sigma}}, \qquad (\hat{r} < 1,\ m_\sigma < \Gamma_\phi), \tag{A.3}$$

where the subscript "osc" denotes the onset of the curvaton oscillation, and Γ_σ and Γ_ϕ are the decay rates of the curvaton and the inflaton, respectively. Here we approximate $\sigma_{\rm osc} \simeq \sigma_*$ by neglecting the curvaton evolution until the onset of its oscillation. Substituting eq. (A.3)

[7] If the curvaton starts to oscillate before the inflaton decays, an extra factor $\sqrt{\Gamma_\phi/m_\sigma}$ is multiplied. Moreover if $\hat{r} > 1$, the expression should be raised to the power of 3/4.

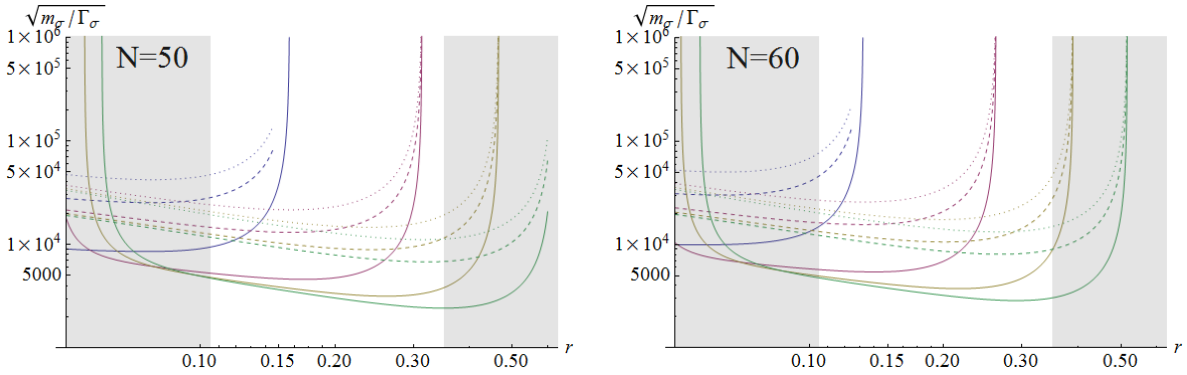

Figure 12. The square root ratio between the curvaton intrinsic mass m_σ and its decay rate Γ_σ. The solid, dashed, dotted lines represent $f_{\rm NL} = 2.7, 8.5, 14.3$, respectively. The colors denotes the chaotic inflation model of $p = 2$ (blue), 4 (red), 6 (yellow) and 8 (green). $m_\sigma < \Gamma_\phi$ is assumed. As $f_{\rm NL}$ increases, $\sqrt{m_\sigma/\Gamma_\sigma}$ also increases because $\sqrt{m_\sigma/\Gamma_\sigma}$ is inversely proportional to $\hat{r} < \mathcal{O}(1)$.

into eq. (4.4), we obtain

$$\sqrt{\frac{m_\sigma}{\Gamma_\sigma}} = \frac{M_{\rm Pl}}{\sigma_*}\frac{24}{2\sqrt{2\epsilon/R} - 3\sigma_*/M_{\rm Pl}}, \tag{A.4}$$

and since σ_* is given in eq. (4.6), $\sqrt{m_\sigma/\Gamma_\sigma}$ can be also explicitly given as a function of ϵ, R and $f_{\rm NL}$. While we omit its complicated expression, fig. 12 shows its value. In fig. 12, one can see that an increasing $f_{\rm NL}$ leads to a larger $\sqrt{m_\sigma/\Gamma_\sigma}$. Apparently, however, this behavior is against the instincts because one may expect that a larger $f_{\rm NL}$ means a smaller $\hat{r}$ and the requirement to boost $\hat{r}$ by the hierarchy between m_σ and Γ_σ is relaxed. Nevertheless, note that eq. (4.4) fixes the relation between $\hat{r}$ and σ_* as $\hat{r} \propto \sigma_*$ for $\hat{r} < \mathcal{O}(1)$. Then eq. (A.3) implies $\sqrt{m_\sigma/\Gamma_\sigma} \propto \hat{r}^{-1}$. Therefore although it seems $\hat{r} \propto \sqrt{m_\sigma/\Gamma_\sigma}$ in eq. (A.3), the actual dependence is in inverse proportion.

In the intrinsic mass curvaton model, $m_{\sigma,\rm eff} = m_\sigma$, we have already computed the m_σ value in eq. (2.18) and fig. 2, and we can obtain Γ_σ explicitly as

$$\Gamma_\sigma = \frac{m_\sigma \sigma_*^2}{576 M_{\rm Pl}^2}\left(2\sqrt{\frac{2\epsilon}{R}} - \frac{3\sigma_*}{M_{\rm Pl}}\right)^2. \tag{A.5}$$

References

[1] K. Enqvist and M. S. Sloth, "Adiabatic CMB perturbations in pre - big bang string cosmology," Nucl. Phys. B **626**, 395 (2002) [hep-ph/0109214].

[2] D. H. Lyth and D. Wands, "Generating the curvature perturbation without an inflaton," Phys. Lett. B **524**, 5 (2002) [hep-ph/0110002].

[3] T. Moroi and T. Takahashi, "Cosmic density perturbations from late decaying scalar condensations," Phys. Rev. D **66**, 063501 (2002) [hep-ph/0206026].

[4] P. A. R. Ade *et al.* [BICEP2 Collaboration], "BICEP2 I: Detection Of B-mode Polarization at Degree Angular Scales," arXiv:1403.3985 [astro-ph.CO].

[5] C. T. Byrnes, M. Corts and A. R. Liddle, arXiv:1403.4591 [astro-ph.CO].

[6] M. S. Sloth, arXiv:1403.8051 [hep-ph].

[7] A. D. Linde, "Chaotic Inflation," Phys. Lett. B **129**, 177 (1983).

[8] A. D. Linde, Contemp. Concepts Phys. **5**, 1 (1990) [hep-th/0503203].

[9] M. Kawasaki, M. Yamaguchi and T. Yanagida, Phys. Rev. Lett. **85**, 3572 (2000) [hep-ph/0004243].

[10] M. Kawasaki, M. Yamaguchi and T. Yanagida, Phys. Rev. D **63**, 103514 (2001) [hep-ph/0011104].

[11] R. Kallosh and A. Linde, JCAP **1011**, 011 (2010) [arXiv:1008.3375 [hep-th]].

[12] R. Kallosh, A. Linde and T. Rube, Phys. Rev. D **83**, 043507 (2011) [arXiv:1011.5945 [hep-th]].

[13] G. Dvali, A. Gruzinov and M. Zaldarriaga, Phys. Rev. D **69**, 023505 (2004) [astro-ph/0303591]l

[14] L. Kofman, astro-ph/0303614;

[15] M. Zaldarriaga, Phys. Rev. D **69**, 043508 (2004) [astro-ph/0306006].

[16] M. Sasaki and E. D. Stewart, Prog. Theor. Phys. **95**, 71 (1996) [astro-ph/9507001];

[17] D. Wands, K. A. Malik, D. H. Lyth and A. R. Liddle, Phys. Rev. D **62**, 043527 (2000) [astro-ph/0003278];

[18] D. H. Lyth, K. A. Malik and M. Sasaki, JCAP **05**,(2005) 004. [astro-ph/0411220].

[19] K. Ichikawa, T. Suyama, T. Takahashi and M. Yamaguchi, Phys. Rev. D **78**, 023513 (2008) [arXiv:0802.4138 [astro-ph]].

[20] K. Enqvist and T. Takahashi, "Mixed Inflaton and Spectator Field Models after Planck," JCAP **1310**, 034 (2013) [arXiv:1306.5958 [astro-ph.CO]].

[21] P. A. R. Ade *et al.* [Planck Collaboration], "Planck 2013 results. XXII. Constraints on inflation," arXiv:1303.5082 [astro-ph.CO].

[22] P. A. R. Ade *et al.* [Planck Collaboration], arXiv:1303.5084 [astro-ph.CO].

[23] T. Kobayashi and T. Takahashi, Phys. Rev. Lett. **110**, 231101 (2013) [arXiv:1303.0242 [astro-ph.CO]].

[24] T. Matsuda, Phys. Lett. B **659**, 783 (2008) [arXiv:0712.2103 [hep-ph]].

[25] T. Kobayashi, F. Takahashi, T. Takahashi and M. Yamaguchi, JCAP **1310**, 042 (2013) [arXiv:1303.6255 [astro-ph.CO]].

[26] E. D. Stewart, Phys. Rev. D **51**, 6847 (1995) [hep-ph/9405389].

[27] M. Dine, L. Randall and S. D. Thomas, Phys. Rev. Lett. **75**, 398 (1995) [hep-ph/9503303].

[28] M. Kawasaki and T. Takesako, Phys. Lett. B **711**, 173 (2012) [arXiv:1112.5823 [hep-ph]].

[29] M. Kawasaki and T. Takesako, Phys. Lett. B **718**, 522 (2012) [arXiv:1208.1323 [hep-ph]].

[30] M. Kawasaki, F. Takahashi and T. Takesako, JCAP **1304**, 008 (2013) [arXiv:1211.4921 [hep-ph]].

[31] A. R. Liddle and D. H. Lyth, Phys. Lett. B **291**, 391 (1992) [astro-ph/9208007].

[32] J. B. Dent, D. A. Easson and H. Tashiro, Phys. Rev. D **86**, 023514 (2012) [arXiv:1202.6066 [astro-ph.CO]].

[33] K. Kohri, Y. Oyama, T. Sekiguchi and T. Takahashi, "Precise Measurements of Primordial Power Spectrum with 21 cm Fluctuations," JCAP **1310**, 065 (2013) [arXiv:1303.1688 [astro-ph.CO]].

[34] D. H. Lyth, C. Ungarelli and D. Wands, Phys. Rev. D **67**, 023503 (2003) [astro-ph/0208055].

[35] M. Kawasaki, T. Kobayashi and F. Takahashi, Phys. Rev. D **84**, 123506 (2011) [arXiv:1107.6011 [astro-ph.CO]].